IEICE TRANS. ELECTRON., VOL. E81-C, NO. 12 DECEMBER 1998

LETTER Special Issue on Computational Electromagnetics

Performance of the Modified PML Absorbing Boundary Condition for Propagating and Evanescent Waves in Three-Dimensional Structures

Zhewang MA†[a)] *and* Yoshio KOBAYASHI†, *Members*

SUMMARY The recently proposed modified PML (MPML) absorbing boundary condition is extended to three dimensions. The performance of the MPML is investigated by FDTD simulation of a typical microstrip line and a rectangular waveguide. The dominant and higher order modes of the microstrip line and the waveguide are excited separately in the computation. In all of the cases of excitation, the reflection properties of the MPML boundaries are examined for the side walls and the end walls, respectively. Various values of the permittivity and permeability of the MPML medium are tested in the computation, and the variation behavior of reflection from the MPML boundaries is examined. The numerical results reveal that by choosing appropriate values of the permittivity and permeability of the MPML, we can realize efficient absorption of both evanescent waves and propagating waves over a wide frequency band.

key words: *FDTD method, absorbing boundary condition, perfectly matched layer (PML), modified PML, evanescent waves*

1. Introduction

The finite-difference time-domain (FDTD) method is being increasingly used to analyze microwave circuits and antennas. As these are typically open region structures, artificial absorbing boundary conditions (ABCs) are usually employed to terminate the computation spaces. High performance absorbing boundaries are of paramount importance to yield accurate and reliable computation results [1].

A number of recent studies reported that in many applications, Berenger's perfectly matched layer (PML) ABC is overwhelmingly superior to other ABCs in absorbing outgoing waves [1]-[3]. It is also found, however, that although Berenger's PML is very effective in absorbing propagating waves, it is ineffective in absorbing evanescent waves [3]-[5]. The reason is that the attenuation rate of an evanescent wave in the PML medium is the same as that in the free space, and the PML does not add any additional attenuation of the wave beyond the natural decaying of the evanescent wave itself.

Manuscript received March 30, 1998.
Manuscript revised June 22, 1998.

† The authors are with the Department of Electrical and Electronic Engineering, Saitama University, Urawa-shi, 338-8570 Japan.
a) E-mail: ma@ees.saitama-u.ac.jp

In order to improve the absorbing efficiency of evanescent waves in the matched layers, a modified PML (MPML) ABC is proposed in two dimensions in [5]. It was demonstrated that by introducing extra degrees of freedom related to the permittivity and permeability of the matched layers, we can make the attenuation rate of evanescent waves in the MPML larger, while the performance for the propagating waves in the MPML is maintained the same as the PML [5].

This paper begins with an extension of the modified PML to three dimensions. The performance of the MPML is then investigated in Sect. 3 by FDTD simulation of a typical microstrip line and a rectangular waveguide. The microstrip line is enclosed by three MPML side walls in the transverse directions, and two MPML end walls in the longitudinal direction. The waveguide is terminated by two MPML end walls in the longitudinal direction. The dominant and higher order modes of the microstrip line and the waveguide are excited separately in the computation. In all of the cases of excitation, the reflection properties of the MPML boundaries are examined for the side walls and the end walls, respectively. Various values of the extra permittivity and permeability of the MPML are tested in the computation, and the variation behavior of reflection from the MPML is examined. It is shown that the attenuation rate of evanescent waves in the MPML is frequency dependent. In general, faster damping of evanescent waves can be obtained by using larger values of the permittivity and permeability of the MPML. However, it is also found that if the values of the introduced permittivity and permeability are too large, large numerical reflections of propagating waves will occur. Therefore, it is usually required to choose appropriate values of the permittivity and permeability in order to realize efficient absorption of both evanescent waves and propagating waves over a wide frequency band.

2. Theory

Maxwell's equations in the three-dimensional modified PML (MPML) are split into twelve equations as follows:

$$\mu_0\mu_y\frac{\partial H_{xy}}{\partial t}+\sigma_y^* H_{xy}=-\frac{\partial(E_{zx}+E_{zy})}{\partial y} \tag{1a}$$

$$\mu_0\mu_z\frac{\partial H_{xz}}{\partial t}+\sigma_z^* H_{xz}=\frac{\partial(E_{yx}+E_{yz})}{\partial z} \tag{1b}$$

$$\mu_0\mu_z\frac{\partial H_{yz}}{\partial t}+\sigma_z^* H_{yz}=-\frac{\partial(E_{xy}+E_{xz})}{\partial z} \tag{1c}$$

$$\mu_0\mu_x\frac{\partial H_{yx}}{\partial t}+\sigma_x^* H_{yx}=\frac{\partial(E_{zx}+E_{zy})}{\partial x} \tag{1d}$$

$$\mu_0\mu_x\frac{\partial H_{zx}}{\partial t}+\sigma_x^* H_{zx}=-\frac{\partial(E_{yx}+E_{yz})}{\partial x} \tag{1e}$$

$$\mu_0\mu_y\frac{\partial H_{zy}}{\partial t}+\sigma_y^* H_{zy}=\frac{\partial(E_{xy}+E_{xz})}{\partial y} \tag{1f}$$

$$\varepsilon_0\varepsilon_y\frac{\partial E_{xy}}{\partial t}+\sigma_y E_{xy}=\frac{\partial(H_{zx}+H_{zy})}{\partial y} \tag{1g}$$

$$\varepsilon_0\varepsilon_z\frac{\partial E_{xz}}{\partial t}+\sigma_z E_{xz}=-\frac{\partial(H_{yx}+H_{yz})}{\partial z} \tag{1h}$$

$$\varepsilon_0\varepsilon_z\frac{\partial E_{yz}}{\partial t}+\sigma_z E_{yz}=\frac{\partial(H_{xy}+H_{xz})}{\partial z} \tag{1i}$$

$$\varepsilon_0\varepsilon_x\frac{\partial E_{yx}}{\partial t}+\sigma_x E_{yx}=-\frac{\partial(H_{zx}+H_{zy})}{\partial x} \tag{1j}$$

$$\varepsilon_0\varepsilon_x\frac{\partial E_{zx}}{\partial t}+\sigma_x E_{zx}=\frac{\partial(H_{yx}+H_{yz})}{\partial x} \tag{1k}$$

$$\varepsilon_0\varepsilon_y\frac{\partial E_{zy}}{\partial t}+\sigma_y E_{zy}=-\frac{\partial(H_{xy}+H_{xz})}{\partial y} \tag{1l}$$

Note that in addition to the conductivities (σ_x, σ_x^*), (σ_y, σ_y^*), and (σ_z, σ_z^*) of Berenger's PML, extra permittivities and permeabilities (ε_x, μ_x), (ε_y, μ_y), and (ε_z, μ_z) are introduced into the above split equations of the modified PML.

By following the procedure similar to that of the two dimensional case [5], the matching condition of the general three-dimensional MPML can be derived as follows:

$$\frac{\sigma_x}{\varepsilon_0}=\frac{\sigma_x^*}{\mu_0},\ \frac{\sigma_y}{\varepsilon_0}=\frac{\sigma_y^*}{\mu_0},\ \frac{\sigma_z}{\varepsilon_0}=\frac{\sigma_z^*}{\mu_0} \tag{2a}$$

$$\varepsilon_x=\mu_x,\ \varepsilon_y=\mu_y,\ \varepsilon_z=\mu_z \tag{2b}$$

When the above matching conditions are satisfied, there should be, theoretically, no reflection at interfaces of the MPML media for incident waves of any frequency and angle. However, in actual numerical computations, reflections will occur due to the contrast of material parameters on the two sides of an interface [2], [3]. In order to minimize the numerical reflections, we define the MPML to be a few cells thick, with the electric conductivity increasing from zero at the free space/MPML interface to a value of σ_{max} at the outer side of the matched layer, and the permittivity varying from unity to a value of $(1+\varepsilon_{max})$. The electric conductivity and the introduced permittivity vary, for example, in the x-direction, in the following forms:

$$\sigma_x(x)=\sigma_{xmax}\left(\frac{x}{\delta}\right)^2 \tag{3a}$$

$$\varepsilon_x(x)=1+\varepsilon_{xmax}\left(\frac{x}{\delta}\right)^2 \tag{3b}$$

here δ is the thickness of the MPML in x-direction. The MPML is backed by a perfect electric conductor (PEC), and the theoretical reflection coefficients for propagating waves and evanescent waves in the MPML are expressed by the following expressions (4a) and (4b), respectively.

$$R_{th}(\varphi)=e^{-\frac{3}{2}\frac{\sigma_{xmax}\delta}{\varepsilon_0 c}\cos\varphi} \tag{4a}$$

$$R'_{th}(\xi)=e^{-2\frac{\omega}{c}(\sinh\xi)\frac{3+\varepsilon_{xmax}}{3}\delta} \tag{4b}$$

where c is the speed of light in the free space, and φ is the angle formed by the wavenumber vector of the propagating wave and the normal to the free space/MPML interface. ξ is a real number larger than zero, and is related to the attenuation rate of the evanescent wave.

From the theoretical reflection coefficient R_{th} of propagating waves at the normal incidence ($\varphi=0$), the maximum value of the conductivity σ_{xmax} can be found as

$$\sigma_{xmax}=-\frac{3\varepsilon_0 c}{2\delta}\ln R_{th} \tag{5a}$$

The value of σ_{xmax} determined by (5a) is a *frequency-independent constant* once R_{th} and δ are given. On the other hand, the maximum value ε_{xmax} of the permittivity can be expressed, by rewritten (4b), as

$$\varepsilon_{xmax}=-3\left[\frac{c}{\omega}\frac{1}{2\delta\sinh\xi}\ln R'_{th}-1\right] \tag{5b}$$

From (5b) we find that the value of ε_{xmax} is *frequency-dependent*. At low frequencies, larger values of ε_{xmax} should be used to realize better absorption of evanescent waves.

Based on the Maxwell's equations (1a)-(1l), the FDTD field update equations in the MPML medium are derived. The standard central-difference scheme is used instead of the exponential time-marching scheme [2], because our numerical tests show that no noticeable difference in numerical results is observed by the two difference schemes.

3. Numerical Results and Discussions

The first structure analyzed in this paper is a microstrip line shown in Fig. 1. The structural parameters are $\varepsilon_r=10.2$, $h=0.635$ mm, and $w=3$ mm. The microstrip line is enclosed by three MPML side walls in the transverse direction, and two MPML end walls in the longitudinal z-direction. The reflection properties of the MPML boundaries are examined for the side walls and end walls, respectively.

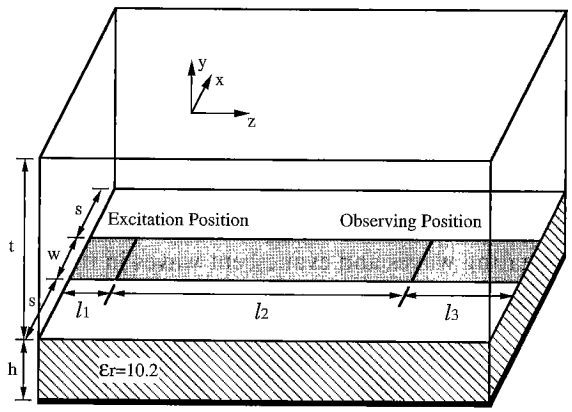

Fig. 1 A microstrip line terminated by MPML boundaries.

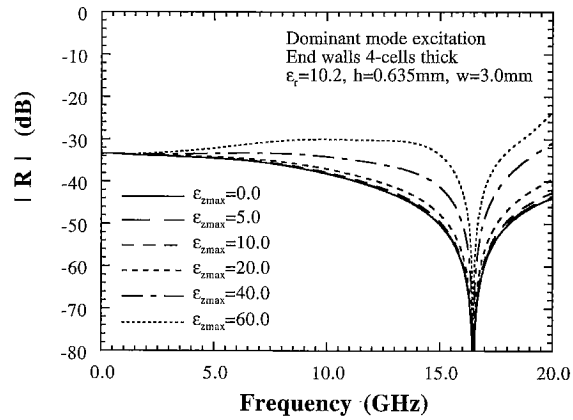

Fig. 2 Performance of the end walls with varying values of ε_{zmax}. The MPML end walls are 4-cells thick with an assigned $R_{th}=10^{-3}$ (−60 dB). The dominant mode of the microstrip line is excited.

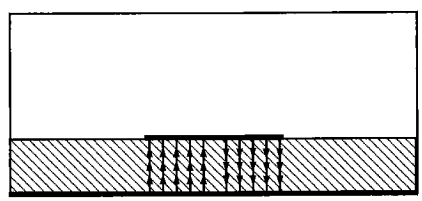

Fig. 3 Excitation of the first higher order mode of the microstrip line by the vertical electric field imposed in an asymmetrical fashion in the excitation plane underneath the metal strip.

The microstrip line shown in Fig. 1 is excitedat a position l_1 away from the left MPML. The time-domain response is recorded at an observing point l_3 away from the right MPML. The distance between the excitation point and the observing point is l_2. The reflection coefficient $|R|$ of the MPML end walls is calculated in two steps. First, the time-domain response of a long microstrip line is calculated as an ideal incident wave reference. The dimensions of this ideal microstrip line are: $w=10\Delta x$, $s=35\Delta x$, $h=5\Delta y$, $t=20\Delta y$, $l_1=40\Delta z$, $l_2=30\Delta z$, and $l_3=50\Delta z$, where $\Delta x=0.3$ mm, $\Delta y=0.127$ mm, and $\Delta z=0.15$ mm, are the grid increments of the FDTD cells. The end walls and side walls of the MPML medium are all 30-cells thick with an assigned $R_{th}=10^{-8}$ and $\varepsilon_x=\varepsilon_y=\varepsilon_z=\mu_x=\mu_y=\mu_z=1$. Next, a shorter microstrip line with $l_1=20\Delta z$, $l_2=30\Delta z$, and $l_3=10\Delta z$ is simulated. This shorter microstrip line has the same MPML side walls of the ideal microstrip line. However, its MPML end walls are varied. We observe the variation of reflection from the MPML end walls by selecting different thickness of the MPML end walls, and by choosing various values of the permittivity ε_{zmax} $(=\mu_{zmax})$ of the MPML end walls.

The microstrip line is first excited by the vertical electric field uniformly imposed in the excitation plane underneath the metal strip. A Gaussian pulse of an effective spectrum width of about 20 GHz is used. The dominant quasi-TEM mode of the microstrip line is excited, which propagates along the microstrip line without cutoff frequency.

Figure 2 depicts the reflection $|R|$ of the MPML end walls with a thickness of 4-cells and an assigned $R_{th}=10^{-3}$ (−60 dB). Different values of the introduced permittivity ε_{zmax} $(=\mu_{zmax})$ are tested in the calculation, and the corresponding $|R|$ are compared. When $\varepsilon_{zmax}=0$, the MPML medium degenerates to Berenger's PML medium. As ε_{zmax} varies from 0 to 20, the reflection varies a little over the whole frequency region. This is expected since the dominant quasi-TEM mode of the microstrip line is a propagating wave in the longitudinal direction over the whole frequency region, and has thereby the same attenuation rate in both the MPML medium and the PML medium. However, when the value of ε_{zmax} becomes larger than 20, extra numerical reflection occurs due to the sharp change of $\varepsilon_z(z)$ and $\mu_z(z)$ between two neighboring cells in the MPML end walls. This results in larger reflection $|R|$, particularly at higher frequencies, as is seen from Fig. 2.

Next we excite the first higher order mode of the microstrip line by imposing the vertical electric field in an asymmetrical fashion in the excitation plane underneath the metal strip, as illustrated in Fig. 3. We get the complex propagation constant of the first higher order mode of the microstrip line by using a mode-matching method [6]–[10]. From the the frequency-dependence of the complex propagation constant, we observed that this first higher order mode has different propagation properties in different frequency regions. When the frequency is greater than about 13.75 GHz, the normalized phase constant β/k_0 is larger than unity, and this frequency region is a bound wave (real spectral) region. When the frequency decreases from 13.75 GHz, the value of β/k_0 becomes smaller than unity. Then, the mode moves from the bound wave region into the leaky wave region. The value of the leakage constant α/k_0 increases quickly with the

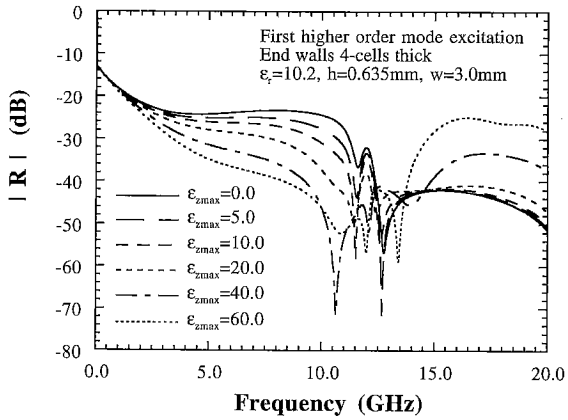

Fig. 4 Performance of the end walls with varying values of ε_{zmax}. The MPML end walls are 4-cells thick with an assigned $R_{th}=10^{-3}$ (−60 dB). The first higher order mode of the microstrip line is excited.

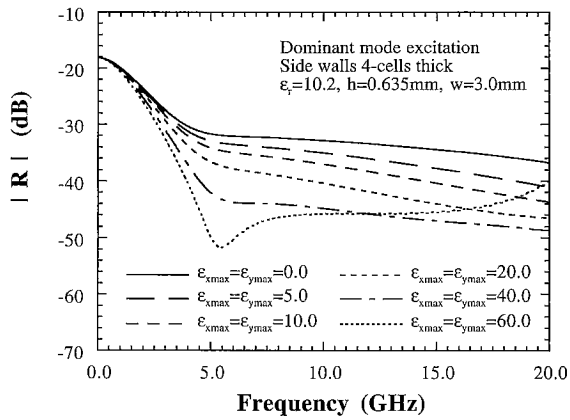

Fig. 5 Performance of the side walls with varying values of ε_{xmax} and ε_{ymax}. The MPML side walls are 4-cells thick with an assigned $R_{th}=10^{-3}$ (−60 dB). The dominant mode of the microstrip line is excited.

decrease of frequency. When the value of α/k_0 becomes quite large, the mode is reactive and below cutoff. In the cutoff frequency region, little leakage of power occurs [6]–[9].

Corresponding to the different propagation properties of the first higher order mode in different frequency regions, the reflection of the first higher order mode by the MPML end walls demonstrates also different behavior in these frequency regions. Figure 4 shows the reflection $|R|$ of the MPML end walls with a thickness of 4-cells and an assigned $R_{th}=10^{-3}$ (−60 dB). When $\varepsilon_{zmax}=0$, the MPML end walls degenerate to PML walls, which are inefficient in absorbing evanescent waves. Therefore, in the cutoff frequency region with $f<10$ GHz, the reflection $|R|$ is quite large, as shown in Fig. 4 by the solid line. In the leaky wave region with $10\text{ GHz}<f<13.75$ GHz, a rapid decrease of $|R|$ is observed, since the leaky wave is a leaky propagating wave and the PML medium becomes more effective. In the bound wave region, the overall reflection is about 20 dB lower than that in the cutoff region. This contrast of reflection level proves the efficiency and inefficiency of the PML medium for propagating and evanescent waves, respectively.

With the increase of the value of ε_{zmax}, the reflection $|R|$ in the cutoff and leaky wave regions is reduced rapidly. At extremingly low frequencies, little improvement in $|R|$ is seen. This can be understood by referring to expression (5b) of Sect. 2, which indicates that at extremingly low frequencies, a very large value of ε_{zmax} should be used for realizing efficient absorption of evanescent waves.

In the bound propagating wave region, only a little variation of $|R|$ is found when the value of ε_{zmax} is increased from 0 to 20. When ε_{zmax} is equal to 40 or 60, $|R|$ increases rapidly in the bound propagating wave region because of the large numerical reflection caused by the sharp change of $\varepsilon_z(z)$ and $\mu_z(z)$ between two neighboring cells in the MPML end walls. The numerical reflection can be alleviated to some extent when the thickness of the end walls is increased.

To examine the reflection properties of the MPML side walls, we make the FDTD simulations in two steps again. First, the time-domain response of a microstrip line with dimensions $w=10\Delta x$, $s=60\Delta x$, $h=5\Delta y$, $t=30\Delta y$, $l_1=15\Delta z$, $l_2=30\Delta z$, and $l_3=25\Delta z$ is calculated as an ideal incident wave reference. The end walls and side walls of the MPML medium are all 30-cells thick with an assigned $R_{th}=10^{-8}$ and $\varepsilon_x=\varepsilon_y=\varepsilon_z=\mu_x=\mu_y=\mu_z=1$. Next, the reflection $|R|$ from the side walls is calculated by moving the three MPML side walls much closer to the metal strip with $s=2\Delta x$, and $t=2\Delta y$. The two MPML end walls remain unchanged. We observe the variation of $|R|$ of the MPML side walls by varying the parameters of these side walls.

Figure 5 indicates $|R|$ of the side walls in the case of the dominant mode excitation, and Fig. 6 in the case of the first higher order mode excitation. In both cases of excitation, waves in the side walls are primarily evanescent, and are exponentially attenuating away in the transverse direction. The only exception is that in the leaky wave frequency region of the first higher order mode, the waves radiate into the MPML side walls.

Since the waves are primarily evanescent in the side walls, the value of $|R|$ in Figs. 5 and 6 reduces with the increase of the value of $\varepsilon_{xmax}=\varepsilon_{ymax}$. This improvement is more obvious at relatively low frequencies. At extremingly low frequencies, little improvement in $|R|$ is seen because of the reason explained in the performance of the MPML end walls. At high frequencies, particularly when the frequency is greater than about 10 GHz, a large value of ε_{xmax} causes large numerical reflections which deteriorate the performance of the MPML side walls.

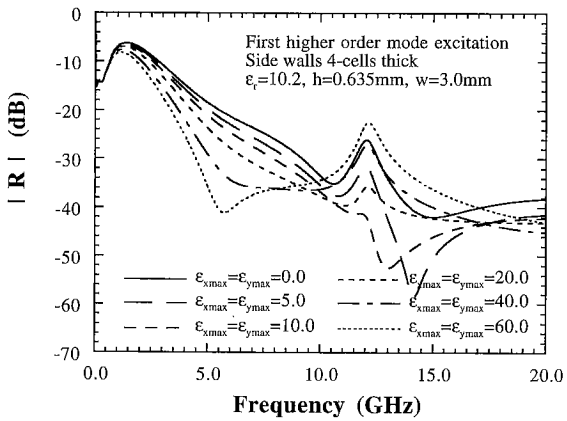

Fig. 6 Performance of the side walls with varying values of ε_{xmax} and ε_{ymax}. The MPML side walls are 4-cells thick with an assigned $R_{th}=10^{-3}$ (−60 dB). The first higher order mode of the microstrip line is excited.

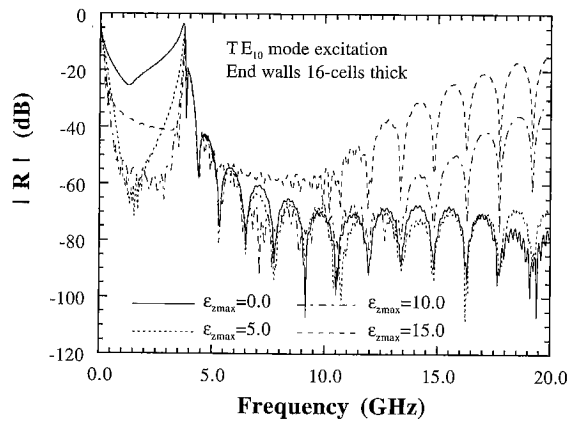

Fig. 8 Performance of the MPML end walls in a rectangular waveguide. The MPML end walls are 16-cells thick with an assigned $R_{th}=10^{-4}$ (−80 dB). TE_{10} mode of the waveguide is excited.

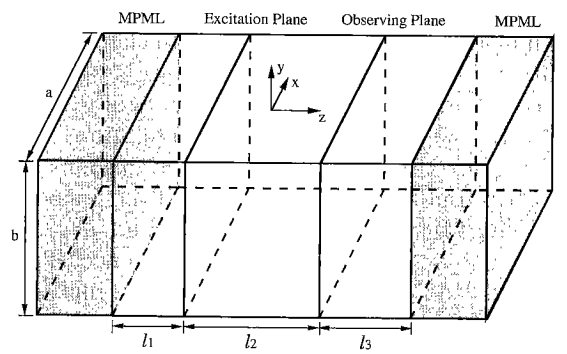

Fig. 7 A rectangular waveguide terminated by two MPML end walls.

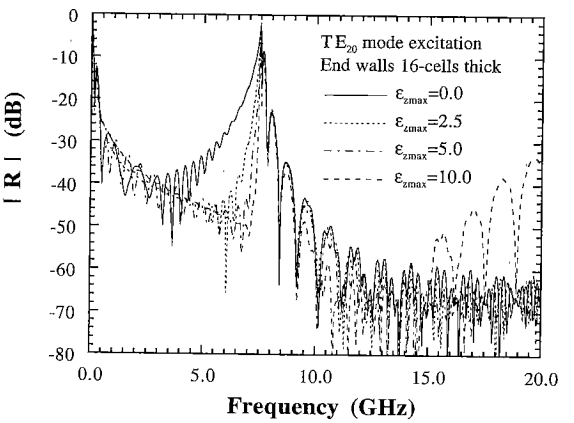

Fig. 9 Performance of the MPML end walls in a rectangular waveguide. The MPML end walls are 16-cells thick with an assigned $R_{th}=10^{-4}$ (−80 dB). TE_{20} mode of the waveguide is excited.

Next we consider a rectangular waveguide filled with free space. The waveguide is terminated by MPML absorbers at the two ends, as shown in Fig. 7. The dimensions of the waveguide are $a=40$ mm and $b=20$ mm. The grid increments of FDTD cells are $\Delta x=\Delta y=\Delta z=1$ mm. The excitation plane and the observing plane are l_1 and l_3 away from the left and right MPML, respectively. The distance between the excitation plane and the observing plane is l_2. As was done for the microstrip line, the reflection from the tested MPML end walls is calculated in two steps. First, the time-domain response of a long waveguide, with $l_1=100\Delta z$, $l_2=20\Delta z$, and $l_3=100\Delta z$, is simulated as an ideal incident wave reference. In order to get an "ideal" reference, the two MPML end walls are set as 64-cells thick with an assigned $R_{th}=10^{-8}$ and $\varepsilon_x=\varepsilon_y=\varepsilon_z=\mu_x=\mu_y=\mu_z=1$. Next, a shorter waveguide with $l_1=100\Delta z$, $l_2=20\Delta z$, and $l_3=1\Delta z$ is simulated. The tested MPML end walls are 16-cells thick with an assigned $R_{th}=10^{-4}$ (−80 dB).

The waveguide is excited by imposing Ey field component in the excitation plane using a function $G(t)\cdot F(x)$, where $G(t)$ is a Gaussian pulse of an effective spectrum width of about 20 GHz, $F(x)$ is a field distribution function. When TE_{10} mode is excited, $F(x)=\sin(\pi x/a)$, and when TE_{20} mode is excited, $F(x)=\sin(2\pi x/a)$. The cutoff frequencies of TE_{10} and TE_{20} modes are 3.75 and 7.5 GHz, respectively.

The reflection from the tested 16-cells thick MPML end walls is investigated by using different values of the permittivity ε_{zmax} of the MPML medium. The obtained reflection coefficients of TE_{10} mode and TE_{20} mode are drawn in Figs. 8 and 9, respectively. When $\varepsilon_{zmax}=0$, the MPML medium degenerates to PML medium. It is seen from Fig. 8 and 9 that the PML ($\varepsilon_{zmax}=0$) provides good absorption of fields in the propagating wave region, but bad performance when the frequency is lower than the cutoff frequency. However, the MPML absorbs efficiently both the propagating and the evanescent waves when the value of ε_{zmax} is not too large. In Fig. 8, when $\varepsilon_{zmax}=10$, the

reflection $|R|$ in the evanescent frequency region is reduced to about -60 dB. However, at frequencies larger than 15 GHz, a relatively large reflection is observed due to the extra numerical reflections occurred among the MPML layers. When ε_{zmax} is further increased to 15, the performance of the MPML is deteriorated in both the propagating and the evanescent frequency regions. In Fig. 9, when ε_{zmax} equals 2.5 or 5.0, the reflection from the MPML is of the same level of that of the PML ($\varepsilon_{zmax}=0$) in the propagating wave region. However, in the evanescent wave region, the MPML has improved reflection property over the PML. If the thickness of the end walls is less than 16-cells, this improvement of reflection will be more significant. When $\varepsilon_{zmax}=10$, the MPML has still much improved performance in the evanescent frequency region. However, it has a larger reflection in the propagating wave region, particularly at high frequencies.

4. Conclusions

The modified PML (MPML) absorbing boundary condition has been extended to three dimensions. The performance of the MPML has been investigated by FDTD simulation of a typical microstrip line and a rectangular waveguide. The dominant and higher order modes of the microstrip line and the waveguide were excited separately in the computation, and the reflection properties of the MPML boundaries were examined for the side walls and end walls, respectively. Different thickness of the MPML and various values of the permittivity and permeability of the MPML were tested in the computation. The variation behavior of reflection from the MPML was examined. The numerical results revealed that by choosing appropriate values of the permittivity and permeability of the MPML, we can realize efficient absorption of both evanescent waves and propagating waves over a wide frequency region.

References

[1] A. Taflove, "Computational Electrodynamics. The Finite-Difference Time-Domain Method," Artech House, Norwood, MA, 1995.

[2] J. P. Berenger, "A perfectly matched layer for the absorption of electromagnetic waves," J. Comput. Phys., vol. 114, pp. 185–200, Oct. 1994.

[3] Z. Wu and J. Fang, "Numerical implementation and performance of perfectly matched layer boundary condition for waveguide structures," IEEE Trans. Microwave Theory & Tech., vol. MTT-43, pp. 2676–2683, Dec. 1995.

[4] J. D. Moerloose and M. A. Stuchly, "Behavior of Berenger's ABC for evanescent waves," IEEE Microwave Guided Wave Lett., vol. 5, pp. 344–346, Oct. 1995.

[5] B. Chen and D. G. Fang, "Modified Berenger PML absorbing boundary condition for FD-TD meshes," IEEE Microwave Guided Wave Lett., vol. 5, pp. 399–401, Nov. 1995.

[6] A. A. Oliner, "Leakage from higher modes on microstrip line with application to antennas," Radio Sci., vol. 22, pp. 907–912, Nov. 1987.

[7] W. T. Lo, C. K. C. Tzuang, S. T. Peng, and C. H. Lin, "Full-wave and experimental investigation of resonant and leaky phenomena of microstrip step discontinuity problems with and without top cover," IEEE MTT-S Int. Microwave Symp. Dig., (San Diego, Cal.), pp. 473–476, 1994.

[8] Z. Ma and E. Yamashita, "Space wave leakage from higher order modes on various planar transmission line structures," IEEE MTT-S Int. Microwave Symp. Dig., (San Diego, Cal.), pp. 1033–1036, 1994.

[9] Y. D. Lin, J. W. Sheen, and C. K. C. Tzuang, "Analysis and design of feeding structures for microstrip leaky wave antenna," IEEE Trans. Microwave Theory & Tech., vol. 44, pp. 1540–1547, Sept. 1996.

[10] Z. Ma and E. Yamashita, "Leakage characteristics of groove guide having a conductor strip," IEEE Trans. Microwave Theory & Tech., vol. 42, pp. 1925–1931, Oct. 1994.